MODELING THE MELTING THRESHOLD OF MO FILMS UPON ULTRASHORT LASER IRRADIATION

KRYSTOF HLINOMAZ[1,2], YOANN LEVY[1], THIBAULT J. Y. DERRIEN[1], NADEZHDA M. BULGAKOVA[1]

[1]HiLASE Centre Institute of Physics ASCR v.v.i.

[2]Czech Technical University in Prague, Faculty of Nuclear Sciences and Physical Engineering

DOI: 10.17973/MMSJ.2019_12_2019104

hlinomazk@fzu.cz

Modification of thin metallic films using ultrashort laser pulses involves interplay of numerous physical processes. Finding a right combination of laser parameters is essential for achieving the desired modification of a thin film deposited on a substrate. Numerical modeling is a convenient tool for gaining insights into ultrafast evolution of material properties and to predict an optimal range of irradiation parameters. In this work, a mathematical model is presented that describes the ultrafast laser heating and temperature relaxation in a thin molybdenum film deposited on a glass substrate. The laser energy absorption by molybdenum is described using a two-temperature model. The model takes into account the heat exchange between the film and the substrate through a boundary condition applied on the lattice temperature. The implicit numerical scheme employed for simulations was verified in respect of energy conservation. The model has been validated by comparison with experimental data on melting threshold fluences.

KEYWORDS

ultrashort laser pulses, thin film, melting threshold, two-temperature model, energy conservation

INTRODUCTION

Laser-matter interaction is a topic that is employed in a wide range of applications in industry. Among the laser parameters, the pulse duration has significant influence on the quality of materials processing, which led to favour the use of ultrashort pulses.

An advantage of shorter laser pulses in respect of longer durations can be clearly seen in ablation of metal targets. The application of fs-pulses results in sharper contours of ablated structure as compared to ps- or ns-pulses [Kautek 1994, Chichkov 1996]. This feature is directly connected with a smaller heat-affected zone (HAZ) caused by shorter pulses [Krause 2017], which is important also for material processing in the vicinity of temperature sensitive structures (such as p-n junctions). The laser processing of a multilayer structures consisting of thin films [Krause 2017] used in photovoltaic industry [Bovatsek 2010] is another demonstrative example.

For performing controlled modifications of thin films, a deep understanding of the involved processes is required that increases the necessity of numerical modeling of laser-matter interaction phenomena which could enable accurate predictions of material evolution. In this paper, a numerical method is presented for determination of the temperature distribution and energy relaxation in a thin molybdenum film after irradiation by single ultrashort laser pulses of 200 fs pulse duration (FWHM) with central wavelength $\lambda = 400$ nm.

In the first section, the physical model of the studied system is presented. The main equations describing laser-induced material heating and the temperature evolution are introduced along with the boundary conditions, description of laser light absorption, and material melting. The temperature-dependent material properties involved in this study are also provided in this section. The second section describes discretization of the equations and the corresponding boundary conditions on a numerical grid. The numerical scheme was developed and implemented in C programming language. Validity of the approach is tested in two steps in the third section: in the first step by controlling the energy conservation and in the second step by the comparison of the computed thickness-dependent melting threshold fluence of Mo films with the experimental data.

1 MODEL

In this section, the thermodynamic model of the studied system (molybdenum film deposited on fused silica substrate) irradiated by a laser pulse is described. A schematic drawing of the system is presented in Fig. 1, summarizing the three main equations, which describe the temperature distribution, and the boundary conditions.

Assuming a laser spot of a sufficiently large size as compared to the optical absorption depth, the transversal heat flow (parallel to the Mo surface) is neglected and the equations can be solved in one dimension. The initial temperature of the whole system is the room temperature (293 K) before the irradiation.

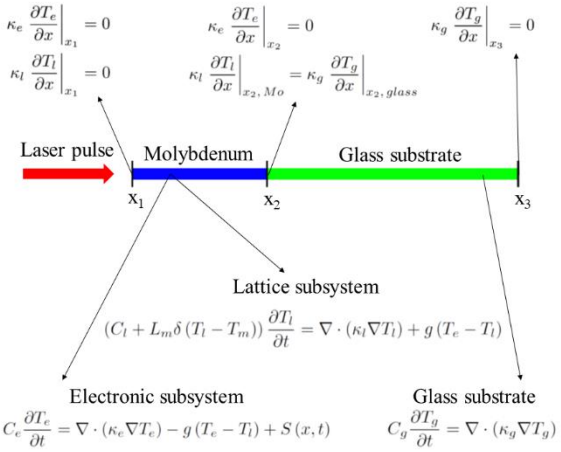

Figure 1. Schematic description of the system modeled, which consists of a thin molybdenum film deposited on the glass substrate. Temperature distribution is described by the three equations at the bottom of the figure, completed by the boundary conditions shown on the top.

1.1 *Equations of the two-temperature model (TTM)*

The two-temperature model is commonly employed for metals, in which free electrons and atomic lattice can be considered as two different but connected subsystems, each with its own temperature [Kaganov 1957, Anisimov 1974, Corkum 1988, Huang 2009]. This description can be particularly handy to address the case of irradiation of solid materials by ultrashort laser pulses. Indeed during an ultrashort pulse action, significantly non-equilibrium situation takes place between electrons (absorbing directly the laser radiation) and the ions of the solid remaining at a temperature comparable to the room temperature. Assuming a local thermal equilibrium, the system

can be described as two subsystems with different temperatures. Each subsystem is assumed thermalized. The advantage of this simplified approach is the possibility to perform relatively fast simulations for the real size of the experimental problem.

The evolution of the temperature of the electronic subsystem $\boldsymbol{T_e}$ is expressed in the form of heat flow equation [Anisimov 1974, Wellershoff 1999]

$$\boldsymbol{C_e \frac{\partial T_e}{\partial t} = \nabla \cdot (\kappa_e \nabla T_e) - g(T_e - T_l) + S}, \qquad (1)$$

where $\boldsymbol{C_e}$ is the heat capacity of electronic subsystem, $\boldsymbol{t}$ is time, $\boldsymbol{\kappa_e}$ is the thermal conductivity of electronic subsystem, $\boldsymbol{T_l}$ is the temperature of the lattice, $\boldsymbol{g = 13 \cdot 10^{16}\ W \cdot m^{-3} \cdot K^{-1}}$ is the electron-phonon coupling factor [Wellershoff 1999] and $\boldsymbol{S}$ the source term describing the absorption of the laser energy. The first term on the right-hand side describes the thermal energy diffusion within the electronic subsystem and the term with the coupling factor $\boldsymbol{g}$ is responsible for heat exchange between two subsystems. The equation for the molybdenum lattice temperature $\boldsymbol{T_l}$ is given by [Anisimov 1974, Wellershoff 1999, Bovatsek 2010]

$$\boldsymbol{\left(C_l + L_m \delta(T_l - T_M)\right) \frac{\partial T_l}{\partial t} = \nabla \cdot (\kappa_l \nabla T_l) + g(T_e - T_l)}, \qquad (2)$$

where $\boldsymbol{C_l}$ is the heat capacity of molybdenum lattice, $\boldsymbol{L_m}$ the latent heat of fusion, $\boldsymbol{\delta}$ is the Dirac delta function used for the description of melting (see section 1.4), $\boldsymbol{T_M}$ is the melting temperature of molybdenum, $\boldsymbol{\kappa_l}$ is the thermal conductivity of the lattice. The first term on the right-hand side stands for the heat diffusion within the lattice subsystem. In this model, the only source of energy received by the lattice is the heat transfer from the electronic subsystem expressed by the electron-phonon coupling factor $\boldsymbol{g}$. The glass substrate is described using a single temperature $\boldsymbol{T_g}$, thus only one heat diffusion equation is needed [Özişik 1980], which is given by

$$\boldsymbol{C_g \frac{\partial T_g}{\partial t} = \nabla \cdot \left(\kappa_g \nabla T_g\right)}. \qquad (3)$$

Here, $\boldsymbol{C_g}$ and $\boldsymbol{\kappa_g}$ are the heat capacity and the thermal conductivity of glass respectively.

1.2 *Boundary conditions*

Zero heat flux boundary conditions [Bovatsek 2010] are applied at the boundaries of the system (see Fig. 1). This means that, at the front surface x_1 of molybdenum (for both electronic and lattice subsystems), the following equations are considered

$$\kappa_e \frac{\partial T_e}{\partial x}\bigg|_{x_1} = 0, \qquad \kappa_l \frac{\partial T_l}{\partial x}\bigg|_{x_1} = 0. \qquad (4)$$

We note that the radiation losses from the film surface are negligible for the considered conditions [Bäuerle 2011].

At the rear surface of the glass substrate x_3, a similar condition is applied which writes as

$$\kappa_g \frac{\partial T_g}{\partial x}\bigg|_{x_3} = 0. \qquad (5)$$

The glass is taken sufficiently thick so that the energy provided by the laser pulse has not enough time to reach the rear surface x_3 during the time of simulations (tens of picoseconds).

Heat transfer between the Mo film and glass is assumed to take place through phonons. To account for the heat flow between the Mo lattice and the substrate these two subsystems are connected by equality of heat flows [Bovatsek 2010], described as

$$\kappa_l \frac{\partial T_l}{\partial x}\bigg|_{x_{2,Mo}} = \kappa_g \frac{\partial T_g}{\partial x}\bigg|_{x_{2,glass}}. \qquad (6)$$

The same temperature is considered at both sides of the interface (the possibility of a temperature jump in the interface is discussed in section 4 together with the effect of the Kapitza resistance) by writing

$$T_l|_{x_{2,Mo}} = T_g|_{x_{2,glass}}. \qquad (7)$$

Because the energy transfer between molybdenum and the glass substrate is provided through the lattice, the boundary condition used for electronic subsystem at the Mo-glass interface is:

$$\kappa_e \frac{\partial T_e}{\partial x}\bigg|_{x_2} = 0. \qquad (8)$$

1.3 *Description of the laser source*

The laser pulse incident on the metal film is described by the intensity $I(t)$ at the front surface. It has a temporal Gaussian shape centered on $t = 2\tau$

$$I(t) = \frac{F}{\tau}\sqrt{\frac{4\ln(2)}{\pi}}\exp\left(-\frac{1}{2}\left(\frac{t-2\tau}{\sigma}\right)^2\right). \qquad (9)$$

In the Eq. (9), F is the incident peak fluence of the laser pulse, τ is pulse duration (FWHM), and σ is the normalization parameter of the Gaussian pulse given by

$$\sigma = \frac{\tau}{2\sqrt{2\ln(2)}}. \qquad (10)$$

Because the objects of interest are thin films, the multilayer reflection (transmission) formula [Stenzel 2005] was used to calculate reflection R and transmission T of the molybdenum film. More precisely, a system composed of three domains was considered: a semi-infinite air region, the Mo thin film of a given thickness, and a semi-infinite glass substrate. The refractive indices and the extinction coefficients of Mo and glass, considered constant, are respectively $n_{Mo,400} = 3.03$, $k_{Mo,400} = 3.22$ [Palik 1998] and $n_{g,400} = 1.522$, $k_{g,400} = 7 \cdot 10^{-8}$ [Khashan 2001]. The obtained reflectivity and transmission were applied at the front surface. The angle of incidence is normal.

In the molybdenum film, the intensity is decaying exponentially with the depth according to the Lambert-Beer law, which results in the source term of the laser energy $S(x,t)$ [Wellershoff 1999], introduced in Eq. (1), given by

$$S(x,t) = I(t) \cdot (1 - R - T) \cdot \frac{\exp\left(-\frac{x}{\lambda_0}\right)}{\lambda_0} \cdot \frac{1}{\left(1 - \exp\left(-\frac{d}{\lambda_0}\right)\right)}, \qquad (11)$$

where d is the thickness of the film and λ_0 is the absorption depth given by

$$\lambda_0 = \frac{1}{\alpha} = \frac{\lambda}{4\pi k_{400}}. \qquad (12)$$

In Eq. (12) α is the absorption coefficient and $\lambda = 400$ nm the wavelength of the laser.

As in [Wellershoff 1999], since both reflection and transmission are already taken into account via the corresponding coefficients R and T, the fraction $\frac{1}{\left(1-\exp\left(\frac{-d}{\lambda_0}\right)\right)}$ is added in Eq. (11) to ensure that, in the model, $\int_0^d S(x,t)\,dx$ is equal to $I(t)\cdot(1-R-T)$ which represents the part of the intensity that is completely absorbed within the metal film.

1.4 Melting

In the Eq. (2) for the lattice subsystem, the term

$$L_m \delta(T_l - T_M)\frac{\partial T_l}{\partial t} \tag{13}$$

accounts for the consumption of the molybdenum melting enthalpy [Bovatsek 2010]. The value of the latent heat of fusion $L_m = 39\,100\ \mathrm{J\cdot mol^{-1}}$, selected on the basis of the comparison of 10 different measurements [Desai 1987], was modified by the molybdenum molar volume $V_{\mathrm{mol}} = 9.334\cdot 10^{-6}\ \mathrm{m^3\cdot mol^{-1}}$ to get $L_m = 2.958\cdot 10^9\ \mathrm{J\cdot m^{-3}}$. The Dirac delta function δ accounts for the latent heat of fusion at the melting temperature of molybdenum $T_M = 2897\ \mathrm{K}$ [Desai 1987] (comparison of 11 references).

1.5 Temperature-dependent material properties

Electronic heat capacity

The temperature-dependent electronic heat capacity of Mo was introduced in the model using four polynomial functions of the orders equal to or less than 4, each in different temperature range. The coefficients in the functions were obtained by careful fitting the data by [Lin 2008, University of Virginia] which are presented in Fig. 2.

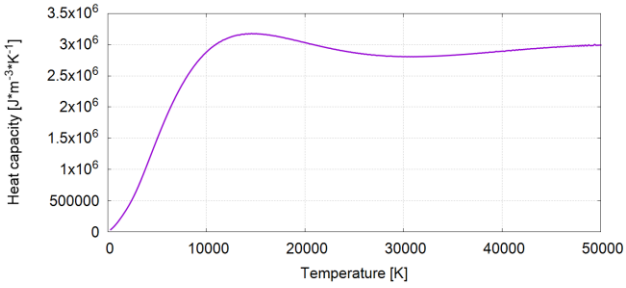

Figure 2. Dependence of the electronic heat capacity C_e of Mo on electronic temperature T_e computed from the first principles [University of Virginia].

Electronic thermal conductivity

The electronic thermal conductivity κ_e is the major part of the total thermal conductivity κ of molybdenum [Wellershoff 1999]. Hence the experimental data on thermal conductivity κ of molybdenum can be used for determination of the parameters applied in the model of the electronic thermal conductivity κ_e. The thermal conductivity of electrons can be expressed by a Drude formulation [Ashcroft 2016] as

$$\kappa_e = \frac{1}{3}v_F^2\frac{C_e}{\nu_{coll}}, \tag{14}$$

where v_F is the Fermi velocity, C_e the heat capacity of electrons and ν_{coll} the collision frequency. The Fermi velocity v_F is obtained according to

$$v_F = \sqrt{\frac{2\cdot E_F}{m_e}} \tag{15}$$

from the Fermi energy $E_F = 6.773$ eV [Bennett 1969] and the mass of electron $m_e = 9.1\cdot 10^{-31}$ kg, which gives the value $v_F \cong 1.544\cdot 10^6\ \mathrm{m\cdot}s^{-1}$.

At temperatures below the Fermi temperature, the collision frequency can be described as the sum of the electron-electron and electron-phonon collision frequencies (using the Matthiessen rule [Ashcroft 2016]) that is described by [Kaveh 1984]

$$\nu_{\mathrm{coll}} = A\cdot T_e^2 + B\cdot T_l\ , \tag{16}$$

where the parameters A and B are assumed to be constant.

The A and B values were determined by rewriting Eq. (14) as

$$\nu_{\mathrm{coll}} = \frac{1}{3}v_F^2\frac{C_e(T)}{\kappa_e(T)}. \tag{17}$$

With experimentally known thermal conductivities $\kappa = \kappa_e$ at given temperatures (in Tab. 1 taken from [Gray 1972] and [Taluts 1988]) and values of the electronic heat capacity C_e introduced above, it is possible to determine A and B.

T [K]	273	373	573	973
κ [W · m^{-1} · K^{-1}]	135	132	130	113

Table 1. Thermal conductivity κ of molybdenum at different temperatures T [Gray 1972].

Indeed the experimental data on the thermal conductivity are measured at thermal equilibrium between the electronic and lattice subsystems, i.e., $T_e = T_l = T$. After obtaining the dependency of the collision frequency ν_{coll} on temperature T from the right hand term of (17), the function (16) was used for fitting the collision frequency ν_{coll} with only one temperature $T = T_e = T_l$ and the parameters A and B were determined.

Fig. 3 shows experimental data on the thermal conductivity κ (taken from [Gray 1972] and [Mills 1996], which also compares the data from references [Filippov 1973, Taluts 1984, Taluts 1988]) and the κ_e value calculated by Eq. (14) assuming $T_e = T_l$ and using the parameters A and B provided by the fitting procedure described above.

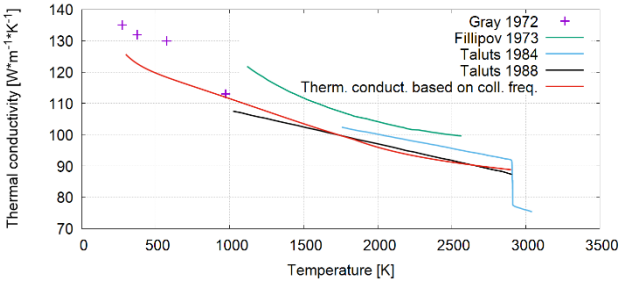

Figure 3. Comparison of the experimental data of the thermal conductivity of molybdenum κ as a function of temperature reported in [Gray 1972, Filippov 1973, Taluts 1984] and [Taluts 1988] with the calculated values based on the collision frequency with the parameters $A = 4.97734\cdot 10^8\ \mathrm{K^{-2}\cdot s^{-1}}$ and $B = 5.90062\cdot 10^{11}\ \mathrm{K^{-1}\cdot s^{-1}}$.

Lattice heat capacity

At temperatures below the melting temperature under normal conditions, the heat capacity of the lattice C_l is considered to be equal to the total heat capacity of molybdenum C. The heat capacity of molybdenum, valid up to its melting point $T_M = 2897$ K, can be expressed as [Chase 1998, NIST]

$$C\ [\mathrm{J\cdot mol^{-1}\cdot K^{-1}}] = A' + B'\cdot T' + C'\cdot T'^2 + D'\cdot T'^3 + \frac{E'}{T'^2}. \tag{18}$$

Here T' is the lattice temperature divided by 1000 e.g. $T' = \frac{T_l}{1000}$. The coefficients of Eq. (18) are listed in the Tab. 2 for two ranges of temperature, 298 – 1900 and 1900 – 2896 K.

To convert Eq. (18) from $\mathrm{J \cdot mol^{-1} \cdot K^{-1}}$ to $\mathrm{J \cdot m^{-3} \cdot K^{-1}}$, the molybdenum molar volume $V_p = 9.334 \cdot 10^{-6}\ \mathrm{m^3 \cdot mol^{-1}}$ was used.

T [K]	298 - 1900	1900 - 2896
A' [$\mathrm{J \cdot mol^{-1} \cdot K^{-1}}$]	24.72736	1231.192
B' [$\mathrm{J \cdot mol^{-1} \cdot K^{-2}}$]	3.960425	-963.4246
C' [$\mathrm{J \cdot mol^{-1} \cdot K^{-3}}$]	-1.270706	283.7292
D' [$\mathrm{J \cdot mol^{-1} \cdot K^{-4}}$]	1.153065	-28.04100
E' [$\mathrm{J \cdot mol^{-1} \cdot K}$]	-0.170246	-712.2047

Table 2. Coefficients in Eq. (18) for the lattice heat capacity [Chase 1998, NIST].

Lattice thermal conductivity

The value of the lattice thermal conductivity κ_l is considered constant and equal to 1 % of the thermal conductivity of the electronic subsystem at room temperature, $\kappa_l = 1.35\ \mathrm{W \cdot m^{-1} \cdot K^{-1}}$ [Wellershoff 1999].

Fused silica thermal conductivity

By fitting the experimental data on thermal conductivity κ_g of fused silica [Carwile 1967], a polynomial function of the third order was derived and employed in the model (see Fig. 4).

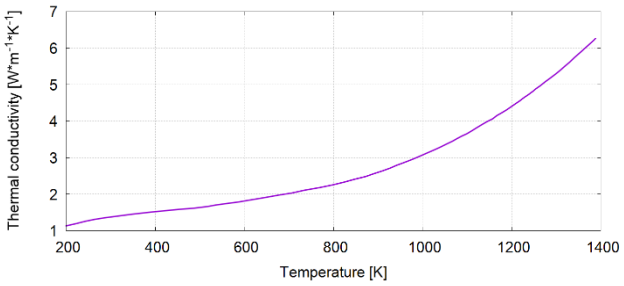

Figure 4. Experimental data on the thermal conductivity κ_g of fused silica (taken from [Carwile 1967]) dependent on temperature T_g.

Fused silica heat capacity

To include the temperature dependence of fused silica heat capacity C_g in the model, the data were adapted from [Bansal 1986].

$$C_g[\mathrm{J \cdot mol^{-1} \cdot K^{-1}}] = 55.98 + 15.4 \cdot 10^{-3} \cdot T_g - 14.4 \cdot 10^{5} \cdot T_g^{-2}. \quad (19)$$

The molar mass $M_{\mathrm{SiO_2}} = 60.06 \cdot 10^{-3}\ kg \cdot \mathrm{mol^{-1}}$ and density of fused silica $\rho_{\mathrm{FS}} = 2.2 \cdot 10^{3}\ kg \cdot \mathrm{m^{-3}}$ were used to express C_g in $\mathrm{J \cdot m^{-3} \cdot K^{-1}}$.

2 NUMERICAL SCHEME

The equations (1), (2) and (3) are solved numerically in one dimension using the finite volume method. The finite volume method involves application of the Gauss divergence theorem (Ostrogradsky theorem) [Mazumder 2016], which is expressed as:

$$\int_V \nabla \cdot \vec{F}\, dV = \oint_S \vec{F} \cdot d\vec{S}. \quad (20)$$

In the other words, the flow of vector field $\vec{F}$ out of volume V through the surface S bounding this volume is equal to the volumetric integral of divergence of the field $\vec{F}$ over the volume V.

First, all three equations (1), (2) and (3) are integrated over the volume of one computational cell which, in this 1D model, is a segment of length $h = 10^{-10}$ m (in this model a regular mesh is used). Then the Gauss theorem is used to eliminate the divergence in the heat diffusion term and the resulting equations are discretized into an implicit numerical scheme.

To build the numerical scheme, we introduce the superscript p and subscript m, which correspond respectively to the number of the time steps from the beginning of the simulation and to the number of a cell in the numerical grid. Then the value of a given quantity Q at the time moment $t = p \cdot \tau$ in the coordinate $x = m \cdot h$ can be written as Q_m^p. In all simulations below, the time step τ is equal to 10^{-15} s.

The electron and lattice temperatures are discretized at the center of each computational cell.

2.1 *Discretization of TTM and heat diffusion equation*

After integration over the computational cell of volume h and application of the Gauss theorem (Eq. (20)), Eq. (1) can be rewritten into the following form

$$h \cdot C_{e,m}^p \frac{T_{e,m}^{p+1} - T_{e,m}^p}{\tau} + \kappa_{e,m-\frac{1}{2}}^p \cdot \frac{T_{e,m}^{p+1} - T_{e,m-1}^{p+1}}{h} - \kappa_{e,m+\frac{1}{2}}^p \cdot \frac{T_{e,m+1}^{p+1} - T_{e,m}^{p+1}}{h} = S_m^p \cdot h - g\left(T_{e,m}^p - T_{l,m}^p\right) \cdot h, \quad (21)$$

where the value of thermal conductivity $\kappa_{e,m-\frac{1}{2}}^p$ determined at the boundary between (m-1)$^{\mathrm{th}}$ and m$^{\mathrm{th}}$ computational cells is calculated as the average value of the thermal conductivities in these cells calculated according to Eq. (14). The thermal conductivity of electronic subsystem $\kappa_{e,m+\frac{1}{2}}^p$ is calculated in the same way between the cells m and (m+1). The Eq. (21) can be rewritten as

$$T_{e,m-1}^{p+1} \cdot \left[-\frac{\kappa_{e,m-\frac{1}{2}}^p}{h}\right] + T_{e,m}^{p+1} \cdot \left[C_{e,m}^p \frac{h}{\tau} + \frac{\kappa_{e,m-\frac{1}{2}}^p}{h} + \frac{\kappa_{e,m+\frac{1}{2}}^p}{h}\right] + T_{e,m+1}^{p+1} \cdot \left[-\frac{\kappa_{e,m+\frac{1}{2}}^p}{h}\right] = S_m^p \cdot h - g\left(T_{e,m}^p - T_{l,m}^p\right) \cdot h + C_{e,m}^p \cdot T_{e,m}^p \frac{h}{\tau}. \quad (22)$$

This equation provides the relation between the temperatures in three consecutive cells $T_{e,m-1}^{p+1}$, $T_{e,m}^{p+1}$, and $T_{e,m}^{p+1}$

$$a_m \cdot T_{m-1}^{p+1} + b_m \cdot T_m^{p+1} + c_m \cdot T_{m+1}^{p+1} = f_m \quad (23)$$

that can be solved by the Thomas (FEBS, Forward Elimination Backward Substitution) algorithm [Godunov 1987].

The heat flow equation for the lattice (Eq. (2)) can be discretized in a similar way

$$h \cdot \left[C_{l,m}^{p} + L_m \delta\left(T_{l,m}^{p} - T_M\right)\right] \frac{T_{l,m}^{p+1} - T_{l,m}^{p}}{\tau} + \kappa_{l,m-\frac{1}{2}}^{p} \cdot \frac{T_{l,m}^{p+1} - T_{l,m-1}^{p+1}}{h} - \kappa_{l,m+\frac{1}{2}}^{p} \cdot \frac{T_{l,m+1}^{p+1} - T_{l,m}^{p+1}}{h} = g\left(T_{e,m}^{p} - T_{l,m}^{p}\right) \cdot h \quad (24)$$

and adjusted to the same form as Eq. (23), that can be again solved by the Thomas algorithm together with the heat diffusion equation for the glass substrate

$$h \cdot C_{g,m}^{p} \frac{T_{g,m}^{p+1} - T_{g,m}^{p}}{\tau} + \kappa_{g,m-\frac{1}{2}}^{p} \cdot \frac{T_{g,m}^{p+1} - T_{g,m-1}^{p+1}}{h} - \kappa_{g,m+\frac{1}{2}}^{p} \cdot \frac{T_{g,m+1}^{p+1} - T_{g,m}^{p+1}}{h} = 0. \quad (25)$$

For practical reasons, the delta function $\delta(T_l - T_M)$ is described by a sufficiently narrow Gaussian function [Zhvavyi 1996]

$$\delta(T_l - T_M, \Delta) = \frac{1}{\sqrt{2\pi}\Delta} \exp\left(-\frac{(T_l - T_M)^2}{2\Delta^2}\right), \quad (26)$$

where Δ is a parameter of Gaussian function governing its shape. The value of Δ must be chosen appropriately. It has to be small enough to keep the Gaussian function similar to the Dirac delta function. However, the Gaussian function should have a width of at least three computational cells [Zhvavyi 1996]. In the present work $\Delta = 1$ K.

2.2 Discretized boundary conditions

The Neumann boundary conditions at the front and rear surfaces, Eqs. (4) and (5), and at the interface for electronic subsystem, Eq. (8), can be implemented by setting the same temperatures in the two cells belonging to the same domain, the boundary cell and the cell adjacent to it. For more precise calculations of the temperature distribution at the interfaces and for better energy conservation in the model, a so-called fictitious cell is added, where the Neumann boundary conditions are applied. In the fictitious cell, the same temperature is set as in the adjacent cell belonging to material.

The situation is more complicated at the interface for describing the heat transport between the lattice subsystem of molybdenum and the glass substrate. For an accurate description of the interface, we introduce the temperature of interface T_{int}^{p+1} and consider the relation between this value and the values of the Mo lattice temperature and the substrate temperature in the cells adjacent to the interface, T_{Mo}^{p+1} and T_{glass}^{p+1} respectively (see Fig. 5).

Discretization of Eq. (6) expressing the conservation of the heat flow at the interface between molybdenum and the substrate can be supplemented by an equation expressing the heat flow between those two adjacent cells directly (assuming that energy is not accumulated at the interface - note that - T_{int}^{p+1} does not belong to any cell). The assumption is that the direct connection between two cells adjacent to the interface can be described by an effective thermal conductivity κ_{eff}^{p}, to be determined. Because the energy is not accumulated at the interface, the following three values of the heat flux must be equal,

$$\kappa_{\text{Mo}}^{p} \frac{T_{\text{int}}^{p+1} - T_{\text{Mo}}^{p+1}}{\frac{h}{2}} = \kappa_{\text{glass}}^{p} \frac{T_{\text{glass}}^{p+1} - T_{\text{int}}^{p+1}}{\frac{h}{2}} = \kappa_{\text{eff}}^{p} \frac{T_{\text{glass}}^{p+1} - T_{\text{Mo}}^{p+1}}{h}. \quad (27)$$

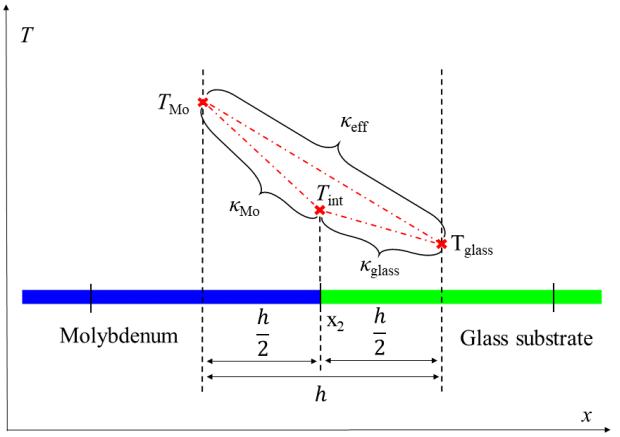

Figure 5. Schematics of the interface between molybdenum and glass substrate.

Note that, in Eq. (27), we use the condition of the equality of the temperature T_{int}^{p+1} at both sides of the interface (as imposed by Eq. (7)). From the equality

$$\kappa_{\text{Mo}}^{p} \frac{T_{\text{int}}^{p+1} - T_{\text{Mo}}^{p+1}}{\frac{h}{2}} = \kappa_{\text{eff}}^{p} \frac{T_{\text{glass}}^{p+1} - T_{\text{Mo}}^{p+1}}{h}, \quad (28)$$

the temperature of the interface can be derived

$$T_{\text{int}}^{p+1} = \frac{\kappa_{\text{eff}}^{p} T_{\text{glass}}^{p+1} - \kappa_{\text{eff}}^{p} T_{\text{Mo}}^{p+1} + 2\kappa_{\text{Mo}}^{p} T_{\text{Mo}}^{p+1}}{2\kappa_{\text{Mo}}^{p}} \quad (29)$$

and eliminated from the second equality of Eq. (27). Thus, the effective heat conductivity κ_{eff}^{p} can be deduced as

$$\kappa_{\text{eff}}^{p} = \frac{2\kappa_{\text{Mo}}^{p} \kappa_{\text{glass}}^{p}}{\kappa_{\text{Mo}}^{p} + \kappa_{\text{glass}}^{p}}. \quad (30)$$

The latter is used in the Thomas algorithm as a common heat conductivity between the last cell of the molybdenum lattice and the first cell of glass. In this way, the Thomas algorithm can be solved via throughout calculations for the lattice subsystem and the substrate.

3 RESULTS

The model described in the section 1 and discretized in the section 2 was applied to the case of laser irradiation of molybdenum thin films deposited on fused silica. The laser pulses of duration $\tau = 200$ fs (FWHM) have a Gaussian form with the central wavelength $\lambda = 400$ nm. Additionally, the case of free-standing molybdenum film was also considered. The model of free-standing film differs from the model of film deposited on substrate by the boundary condition at the remote film boundary. At the interface x_2, the Eq. (6) and (7) were replaced by the Neumann boundary condition for the lattice system, similar to the one for electrons (Eq. (8)) instead of the conditions at the Mo-glass interface. Additionally, the third layer (glass) in multilayer model of reflectivity (see section 1.3) was substituted by air for accurate calculations of the reflection and transmission coefficients.

In this section, the results provided by the model are compared with the experimental data on melting threshold and the energy conservation of the model is discussed.

3.1 *Energy conservation*

The conservation of the laser energy was controlled during the simulation.

Fig. 6 shows the evolution of the energy in different subsystems in the case of molybdenum film of thickness 25 nm deposited on glass substrate and irradiated by the laser pulse with the incident fluence $74\ \mathrm{mJ \cdot cm^{-2}}$ corresponding to the calculated melting threshold. The melting threshold was determined to be the lowest fluence leading to complete melting of the first numerical cell, i.e. when the melting enthalpy is fully consumed in this cell.

In Fig. 7 the same information is plotted for the case of a free-standing molybdenum film of thickness 60 nm and irradiated by laser pulse with incident fluence $98\ \mathrm{mJ \cdot cm^{-2}}$ corresponding to the calculated melting threshold in this case.

Comparison of the absorbed laser energy (light blue solid lines) with total energy (red dashed line) in the materials (in Mo film and glass for Fig. 6, in free-standing Mo film for Fig. 7) confirms that energy is conserved during computation with high accuracy in both cases with and without the substrate. The energy of electrons (green dashed lines), which is increasing abruptly as the light is absorbed during the ultrashort laser pulse, is then dropping due the electron-phonon coupling and corresponding thermalization between electronics and lattice subsystems. The curve for Mo lattice energy in both figures accounts for the energy consumed for lattice heating and the curve labeled 'Melting energy' (black dashed line) corresponds to the consumption (upon melting) and release (upon solidification) of the melting enthalpy. The heat transport through the Mo-glass interface increases energy in the substrate with time while the film is gradually cooling as can be seen in Fig. 6.

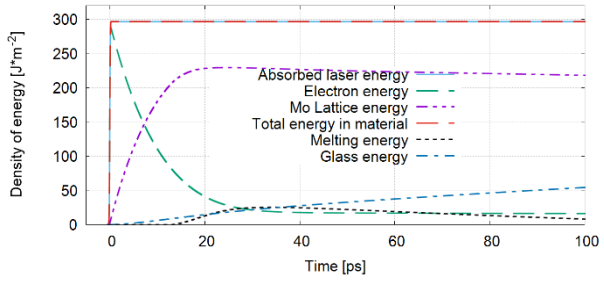

Figure 6. Temporal evolution of the energy in different subsystems of the molybdenum film of thickness 25 nm deposited on fused silica. The film was irradiated by a laser pulse (λ = 400 nm, τ = 200 fs (FWHM)). The incident laser fluence of $74\ \mathrm{mJ \cdot cm^{-2}}$ corresponds to the calculated melting threshold (complete melting of the surface cell of the film).

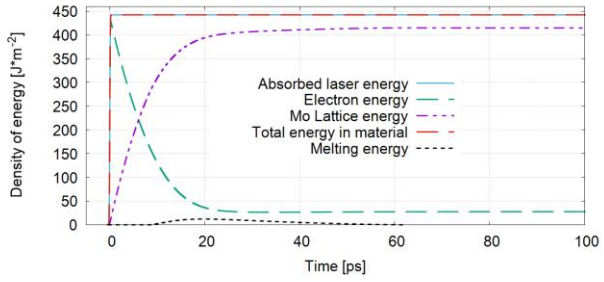

Figure 7. Temporal evolution of the energy in different subsystems of the molybdenum free-standing film of thickness 60 nm. The film was irradiated by a laser pulse (λ = 400 nm, τ = 200 fs (FWHM)). The incident laser fluence of $98\ \mathrm{mJ \cdot cm^{-2}}$ corresponds to the calculated melting threshold.

3.2 *Comparison with experimental data*

The aim is to reproduce the experimentally observed dependence of the absorbed fluence corresponding to the melting threshold as a function of the Mo film thickness. Two sets of simulations were prepared, one with the molybdenum films deposited on substrate and another one with the molybdenum free-standing films. The results of both simulations are shown in Fig. 8 together with the experimental data [Wellershoff 1999].

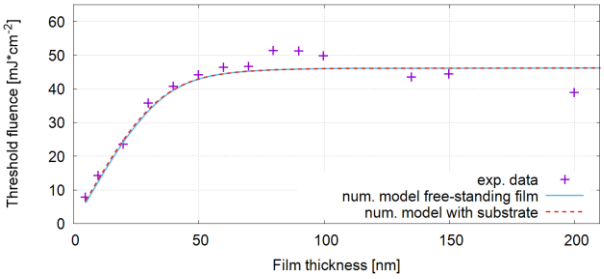

Figure 8. Absorbed fluence corresponding to the melting threshold for the Gaussian laser pulse (λ = 400 nm, τ = 200 fs (FWHM)) as function of molybdenum film thickness. Numerical simulations were performed for free-standing films and films deposited on the substrate (fused silica). Experimental data are taken from [Wellershoff 1999].

From Fig. 8 it is clearly seen that both models (for molybdenum films with and without substrate) reproduce very well the experimental data on melting threshold fluence in the range of experimentally investigated thicknesses.

For the relatively thick films ($d > 50\ \mathrm{nm}$), the melting threshold fluence is saturating and film melting behaves as the case of bulk irradiation. For thinner films ($d < 50\ \mathrm{nm}$), the melting threshold fluence is decreasing with decreasing film thickness. The change of the threshold fluence tendency from thin film to the bulk behavior is observed around 50 nm in both numerical and experimental data.

4 DISCUSSION

According to the results shown in the previous section, the developed numerical model is capable of providing values of the melting threshold fluence for molybdenum films, which are in very good agreement with the experimental data (see Fig. 8). The numerical scheme conserves the energy with a high precision during the simulations (see Figs. 6 and 7) for films of different thicknesses. However, several points in our approach need discussion.

It is reasonable to assume that the model can be successfully applied to the cases of irradiation by the laser pulse ($\lambda = 400\ \mathrm{nm}$, $\tau = 200\ \mathrm{fs\ (FWHM)}$) with lower fluences than the calculated melting threshold. However, we neglect here a possible damage caused by stress. It should be noted that the damage threshold fluence can occur to be lower than the melting threshold due to mechanical effects like microcracks caused by thermally-induced stress [Domke 2014].

To apply the two-temperature model, the temperature must be already established in each subsystem. However, at very short time periods, during or right after ultrashort laser pulse irradiation, the electronic subsystem may not have been thermalized yet [Rethfeld 2002]. However, good agreement with the experimental data supports the assumption of minor

influence of the processes related to the mentioned situation, at least for molybdenum in the irradiation regime described here.

Radiation losses due to the emissivity of the front surface of the thin film [Honnerová 2017] was neglected. The energy loss by thermal radiation during the simulation time (up to melting) is negligibly small as compared to the energy absorbed by the film and dissipated in the film-substrate system. For longer times, the emissivity can play more important role and can be added as a part of source term.

Some material properties were not considered as dependent on temperature (e.g., the electron-phonon coupling factor g and refractive index). Their temperature dependences can be taken into account in future to possibly improve the model. Regarding the electron-phonon coupling factor, some questions have emerged recently on the use of the temperature-dependent coupling factor when addressing even stronger regimes of irradiation of thin metallic films [Mo 2018, Sokolowski-Tinten 2015]. The temperature dependence of optical properties can have an effect on the reflection and transmission [Gnilitskyi 2017]. However, the latter dependence will be more important for laser intensities well higher the melting threshold (in the regimes of strong ablation).

Another important point to underline is that all material properties involved in the model presented here, except for coupling factor g, are for bulk material. It was shown however [Alvarez 2007] that confinement effects could affect the transport properties. The influence of the effects of confinement on the melting threshold of thin films of different thicknesses will be analyzed in our future works.

Finally, the assumption of the equality of the temperature of molybdenum and glass in the interface between them and the possible effect [Swartz 1989] of the Kapitza resistance is questionable. The boundary condition between the lattice subsystem and glass described in this paper can be considered as condition with the Kapitza resistance equal to zero whereas the simulations of the free standing films correspond to the case of the infinite resistance at the interface. Since no visible effect can be seen on the results presented on Fig. 8, the modeled configuration seems to be unaffected by such phenomenon. Other systems, however, e.g. with substrates of higher thermal conductivity like silicon or metals, would require further implementation of this resistance.

Also there is a possibility of another energy channel between molybdenum and glass substrate mentioned in several recent studies (for example in [Guo 2012]). Its principle lies in the direct coupling of the electronic subsystem with glass. This could lead to increase of the heat flux through the molybdenum-glass interface.

5 CONCLUSIONS

A thermodynamic model of laser energy absorption by molybdenum films was developed. The cases of free-standing films and of films deposited on a fused silica substrate irradiated with ultrashort laser pulses were investigated. The model's equations were discretized and a numerical code was prepared based on C programming language. It was verified that the energy was conserved during the simulations with high accuracy. The calculated melting threshold fluences of molybdenum films of different thicknesses on glass substrates are in good agreement with the available experimental data of femtosecond laser-induced melting threshold.

ACKNOWLEDGMENTS

This work was supported by the European Regional Development Fund and the state budget of the Czech Republic (Project No. BIATRI: CZ.02.1.01/0.0/0.0/15_003/0000445), the Ministry of Education, Youth and Sports of the Czech Republic (Programmes NPU I Project No. LO1602, and the Large Research Infrastructure Project No. LM2015086). K.H. also acknowledges the support of the Grant Agency of the Czech Technical University in Prague (No. SGS19/191/OHK4/3T/14).

REFERENCES

[Alvarez 2007] Alvarez, F. and Jou, D. Memory and nonlocal effects in heat transport: from diffusive to ballistic regimes. Applied Physics Letters, 2007, Vol. 90, No. 8, id. 083109, pp 1-3

[Anisimov 1974] Anisimov, S.I., et al. Electron emission from metal surfaces exposed to ultrashort laser pulses. Soviet Physics - JETP, August 1974, Vol. 39, No. 2, pp 375-377

[Ashcroft 2016] Ashcroft, N.W., et al. Solid State Physics. Singapore: Cengage, 2016. ISBN-13 978-981-4369-89-3

[Bansal 1986] Bansal, N.P. and Doremus, R.H. Handbook of Glass Properties. Orlando: Academic Press., 1986. ISBN 0-12-078140-9

[Bäuerle 2011] Bäuerle, D. Laser Processing and Chemistry 4th ed. London: Springer., 2011. ISBN 978-3-642-17613-5

[Bovatsek 2010] Bovatsek, J., et al. Thin film removal mechanisms in ns-laser processing of photovoltaic materials. Thin Solid Films, 2010, Vol. 518, No. 10, pp 2897-2904

[Bulgakova 2010] Bulgakova, N.M., et al. Laser-induced modification of transparent crystals and glasses. Quantum Electronics, 2010, Vol. 40, No. 11, pp 966-985

[Carwile 1967] Carwile, L.C.K. and Hoge, H.J. Thermal Conductivity of Vitreous Silica: Selected Values. In: D.R. Flynn and B.A. Peavy Jr., ed. Thermal conductivity: proceedings of the seventh conference held at the National Bureau of Standards, Gaithersburg, Maryland, 1967, pp 59-76

[Chase 1998] Chase, M.W., Jr. NIST-JANAF Thermochemical Tables 4th ed., Journal of Physical and Chemical Reference Data, 1989, Monograph 9, pp 1-1951

[Chichkov 1996] Chichkov, B.N., et al. Femtosecond, picosecond and nanosecond laser ablation of solids. Applied Physics A, 1996, Vol. 63, No. 2, pp 109-115

[Corkum 1988] Corkum, P.B., et al. Thermal Response of Metals to Ultrashort-Pulse Laser Excitation. Physical Review Letters, 1988, Vol. 61, No. 25, pp 2886-2889

[Desai 1987] Desai, P.D. Thermodynamic Properties of Manganese and Molybdenum. Journal of Physical

and Chemical Reference Data, 1987, Vol. 16, No. 1, pp 91-108

[Domke 2014] Domke, M., et al. Understanding thin film laser ablation: The role of the effective penetration depth and the film thickness. In: M. Schmidt, ed. Physics Procedia, 8th International Conference on Laser Assisted Net Shape Engineering LANE, Fürth, 2014, Vol. 56, pp 1007-1014

[Filippov 1973] Filippov, L.P. Untersuchung der thermischen Eigenschaften im Stoff an der Moskauer Universität. International Journal of Heat and Mass Transfer, 1973, Vol. 16, No. 5, pp 865-885

[Gnilitskyi 2017] Gnilitskyi, I. et al. High-speed manufacturing of highly regular femtosecond laser-induced periodic surface structures: physical origin of regularity. Scientific Reports, 2017, Vol. 7, 8485 pp 1-11

[Godunov 1987] Godunov, S.K. and Ryabenkii, V.S. Difference Schemes. Amsterdam: Elsevier., 1987. ISBN 0-444-70233-4

[Guo 2012] Guo, L., et al. Heat Transfer Across Metal-Dielectric Interfaces During Ultrafast-Laser Heating. Journal of Heat Transfer, 2012, Vol. 134, No. 4, id. 042402, pp 1-5

[Gray 1972] Gray, D.E. American Institute of Physics Handbook 3rd ed. New York: McGraw-Hill., 1972. ISBN 978-0070014855

[Honnerová 2017] Honnerová, P., et al. Method for emissivity measurement of semitransparent coatings at ambient temperature. Scientific Reports, 2017, Vol. 7, 1386 pp 1-14

[Huang 2009] Huang, J., et al. Ultrafast solid-liquid-vapor phase change of a gold film induced by pico- to femtosecond lasers. Applied Physics A, 2009, Vol. 95, No. 3, pp 643-653

[Kaganov 1957] Kaganov, M.I., et al. Relaxation between Electrons and the Crystalline Lattice. Soviet Physics - JETP, 1957, Vol. 4, No. 2, pp 173-178,

[Kautek 1994] Kautek, W. and Krueger, J. Femtosecond pulse laser ablation of metallic, semiconducting, ceramic, and biological materials. In: E. Beyer, ed. Proceedings of the SPIE, Europto High Power Lasers and Laser Applications V, Laser Materials Processing: Industrial and Microelectronics Applications, Vienna, 1994, Vol. 2207, pp 600-611

[Kaveh 1984] Kaveh, M. and Wiser, N. Electron-electron scattering in conducting materials. Advances in Physics, 1984, Vol. 33, No. 4, pp 257-372,

[Khashan 2001] Khashan, M.A. and Nassif, A.Y. Dispersion of the optical constants of quartz and polymethyl methacrylate glasses in a wide spectral range: 0.2-3 µm. Optics Communications, 2001, Vol. 188, No. 1-4, pp 129-139,

[Krause 2017] Krause, S., et al. Layer-selective laser-lift off and removal mechanism in a TCO/Si thin film system by nano- to femtosecond pulses. In: Proceedings of Lasers in Manufacturing Conference, Munich, 2017, pp 1-11

[Lin 2008] Lin, Z., et al. Electron-phonon coupling and electron heat capacity of metals under conditions of strong electron-phonon nonequilibrium. Physical Review B, 2008, Vol. 77, No. 7, id. 075133, pp 1-17

[Mazumder 2016] Mazumder, S. Numerical Methods for Partial Differential Equations Finite Difference and Finite Volume Methods. London: Academic Press., 2016. ISBN 978-0-12-849894-1

[Mills 1996] Mills, K.C., et al. Thermal conductivities of molten metals: Part 1 Pure metals. International Materials Reviews, 1996, Vol. 41, No. 6, pp 209-242

[Mo 2018] Mo, M.Z., et al. Heterogeneous to homogeneous melting transition visualized with ultrafast electron diffraction. Science, 2018, Vol. 360, No. 6396, pp 1451-1455

[NIST] molybdenum, NIST, [online]. [29.9.2019]. https://webbook.nist.gov/cgi/cbook.cgi?ID=C7439987&Mask=2#Thermo-Condensed

[Özişik 1980] Özişik, M.N. Heat conduction. New York: John Wiley & Sons, 1980. ISBN 0-471-05481-X

[Palik 1998] Palik, E.D. Handbook of Optical Constants of Solids. London: Academic Press, 1998. ISBN 0-12-544420-6

[Petroff 1969] Petroff, I. and Viswanathan, C.R. Calculation of Density of States in W, Ta, and Mo. In: L.H. Bennett, ed. Electronic density of states: Based on Invited and Contributed Papers and Discussion 3rd Materials Research Symposium, Gaithersburg, Maryland, 1969. Publisher, pp 53-56

[Rethfeld 2002] Rethfeld, B., et al. Ultrafast dynamics of nonequilibrium electrons in metals under femtosecond laser irradiation. Physical Review B, 2002, Vol. 65, No. 21, id. 214303, pp 1-11

[Sokolowski-Tinten 2015] Sokolowski-Tinten, K., et al. Thickness-dependent electron-lattice equilibration in laser-excited thin bismuth films. New Journal of Physics, 2015, Vol. 17, No. 11, id. 113047, pp 1-9

[Stenzel 2005] Stenzel, O. The Physics of Thin Film Optical Spectra. Berlin: Springer., 2005. ISBN-10 3-540-23147-1

[Swartz 1989] Swartz, E.T. and Pohl, R.O. Thermal boundary resistance. Reviews of Modern Physics, 1989, Vol. 61, No. 3, pp 605-668

[Taluts 1984] Taluts, S.G. et al. Temperature and heat conductivities of solid and liquid molybdenum. Fyzika metallov i metallovedenie, 1984, Vol. 58, No. 3, pp 617-619 (in Russian)

[Taluts 1988] Taluts, S.G. et al. Temperature and thermal conductivity of high-purity refractory metal

monocrystals from 1000 K to melting point. Vysokochistye Veshchestva, 1988, Vol. 3, pp 208-211 (in Russian)

[University of Virginia] Electron-Phonon Coupling and Electron Heat Capacity in Metals at High Electron Temperatures., University of Virginia, [29.9.2019]. http://www.faculty.virginia.edu/CompMat/electron-phonon-coupling/

[Wellershoff 1999] Wellershoff, S.S., et al. The role of electron-phonon coupling in femtosecond laser damage of metals. Applied Physics A, 1999, Vol. 69, No. 1 Supplement, pp S99-S107

[Zhvavyi 1996] Zhvavyi, S.P. and Ivlev, G.D. Influence of the initial temperature of silicon on crystallization of a layer melted by nanosecond laser heating. Journal of Engineering Physics and Thermophysics, 1996, Vol. 69, No. 5, pp 608-611

CONTACTS:

Ing. Krystof Hlinomaz

Yoann Levy, Ph.D.

Thibault J.-Y. Derrien, Ph.D.

Prof. Dr. Sci. Nadezhda M. Bulgakova, Ph.D.

HiLASE Centre, Institute of Physics of the Czech Academy of Sciences

Za Radnici 828, Dolní Brezany 252 41 , Czech Republic

+420 314 007 754, hlinomazk@fzu.cz, www.hilase.cz